

Temperature Rise in 3D Anisotropic Layered Structures in Thermoreflectance and 3ω Experiments

Puqing Jiang,^{1,2,a)} and Heng Ban^{1,2,b)}

¹*Department of Mechanical Engineering and Materials Science, University of Pittsburgh, Pittsburgh, Pennsylvania 15261, USA*

²*Pittsburgh Quantum Institute, Pittsburgh, Pennsylvania 15260, USA*

Abstract

Recent developments of transient thermal measurement techniques including the thermoreflectance methods (time-domain/frequency-domain thermoreflectance, TDTR/FDTR) and the 3ω method enabled measurements of anisotropic thermal conductivities of bulk and thin film materials. Estimating the temperature rise of anisotropic layered structures under surface heating is critically important to make sure that the temperature rise is not too high to alias the signals in these experiments. However, a simple formula to estimate the temperature rise in 3D anisotropic layered systems is not available yet. In this work, we provide simple analytical expressions to estimate the peak temperature rise in anisotropic layered structures for the cases of both laser heating (as in thermoreflectance experiments) and metal strip heating (as in 3ω experiments). We started by solving the 3D anisotropic heat diffusion equation in the frequency domain for a multilayered structure and derived a general formalism of the temperature rise. This general formalism, while normally requiring numerical evaluation, can be reduced to simple analytical expressions for the case of semi-infinite solids. We further extended these analytical expressions to multilayered systems, assuming linear temperature gradients within the thin layers above the semi-infinite substrates. These analytical expressions for multilayered systems are compared with the exact numerical solutions of the heat diffusion equation for several different cases and are found to

^a jiangpq04@gmail.com

^b heng.ban@pitt.edu

work generally well but could overestimate the temperature rise in some special occasions. These simple analytical expressions serve the purpose of estimating the maximum temperature rise of 3D anisotropic layered systems, which greatly benefits the thermoreflectance and 3ω experiments in choosing the appropriate heating power and heater sizes for the experiments.

Keywords: *Temperature rise; 3D anisotropic; thermoreflectance; 3ω method*

1. Introduction

Thermal conductivity of thin films is a critical property that impacts their wide applications in modern devices such as microelectronics,¹ photonics,² solar cells,³ thermal barrier coatings⁴ and thermoelectric modules.⁵ Accurate measurements of the thermal conductivity of thin films and small-scale samples were made possible with the recent development of transient techniques including the thermoreflectance methods (time-domain/frequency-domain thermoreflectance, TDTR/FDTR) and the 3ω method. These techniques have been extensively used to measure the thermal conductivity of both thin films and bulk materials over a wide range of thermal conductivity.^{6,7}

Both the thermoreflectance methods and the 3ω method rely on periodic heating of the sample on the surface and detecting the resulted temperature oscillation to derive the thermal conductivity of the sample, although using different schemes. The thermoreflectance methods use a modulated laser beam to heat the sample and a second laser beam to detect the surface temperature change via the linear change of the surface reflectance R_s with temperature, $\Delta R_s = \frac{dR_s}{dT} \Delta T$. On the other hand, in the 3ω method, the sample is heated by supplying a modulated Joule heating to a metal strip deposited on the sample surface, and the corresponding temperature change of the sample surface is monitored through the linear

change of the electrical resistance R_e of the metal strip with temperature, $\Delta R_e = \frac{dR_e}{dT} \Delta T$. In both cases, the surface temperature rise ΔT should not be too high to invalidate the assumption of linear temperature dependence of R_s and R_e . Besides, since both methods measure the thermal properties of the sample at the base temperature T_0 , the surface temperature rise ΔT should not be too high to invalidate the assumption of temperature-independent thermal properties. This is particularly important at low temperatures where the heat capacities have the T^3 temperature dependence. A general guideline is that the surface temperature rise ΔT should not exceed 10 K or 10% the absolute temperature, whichever is smaller.^{6,8} A quick and accurate estimation of the temperature rise in both thermoreflectance and 3ω experiments is thus critically important in choosing an appropriate heating power and heater size for these experiments.

Although the useful signals in thermoreflectance and 3ω experiments are induced by the periodic heating, the surface heat flux inevitably contains a constant offset component, and the amplitude of the constant offset component is always larger than or equal to that of the periodic component of the heat flux, see Fig. 1(a) for an illustration. There are thus two components in the temperature rise of the sample: a steady-state temperature rise induced by the constant offset of the heat flux and a steady periodic temperature oscillation induced by the periodic component of the heat flux (see Fig. 1(b)). As will be demonstrated later, the amplitude of the steady-state temperature rise only depends on the thermal conductivity of the sample, but the amplitude of the periodic temperature oscillation also depends on the heat capacity of the sample and the oscillating frequency of the heat flux. Since the amplitude of the steady-state temperature rise is always larger than or equal to that of the periodic temperature oscillation, one only needs to estimate the steady-state temperature rise and make sure that it is not too high, and then the amplitude of the periodic temperature oscillation will certainly be within the acceptable range.

For the thermoreflectance experiments, Cahill⁹ was the first to derive an analytical expression to estimate the steady-state temperature rise of an isotropic semi-infinite solid, which was later extended to a more general form by Braun *et al.*¹⁰ as

$$\Delta T = \frac{A_0}{\sqrt{2\pi k_z k_r (w_0^2 + w_1^2)}}. \quad (1)$$

Here, A_0 is the laser power absorbed by the sample, k_r and k_z are the in-plane and through-plane thermal conductivities of the material, w_0 and w_1 are the $1/e^2$ radii of the pump and probe laser spots, and ΔT is the temperature rise as averaged by the probe beam. While Eq. (1) has been commonly used in TDTR/FDTR experiments to estimate the temperature rise, it is limited to specific cases where both the in-plane thermal conductivity and the laser spot size need to be axially symmetric. In addition, as pointed out by Braun *et al.*¹⁰, the layers and interfaces in multilayered systems could possibly redistribute the heat flux and result in a temperature rise that is different from the one predicted using Eq. (1), which is for semi-infinite solids. Unfortunately, a metal transducer layer is usually indispensable in TDTR/FDTR experiments, inevitably making the sample structure a multilayered one. Besides, there are many occasions where the measurements of thin films on a substrate are desired. A more general formulation for the temperature rise that can apply to multilayered systems with 3D anisotropy is urgently needed.

For the 3ω experiments, deriving an analytical expression for the temperature rise is more difficult because the heater size lacks the axial symmetry. Cahill¹¹ provided an expression

$$\Delta T = \frac{A_0}{\pi L k} \int_0^\infty \frac{\sin^2(b\lambda/2)}{(b\lambda/2)^2 \sqrt{\lambda^2 + i\omega_0 C/k}} d\lambda \quad (2)$$

for the surface temperature rise of an isotropic semi-infinite solid when the metal strip was supplied with an AC current at frequency $\omega_0/2$, which produces a periodic heat flux at the frequency ω_0 . Here, L and b are the length and the width of the metal strip, respectively, k

and C are the thermal conductivity and volumetric heat capacity of the isotropic semi-infinite solid, and the temperature is averaged across the metal strip width. Borca-Tasciuc *et al.*¹² further extended Eq. (2) to be applicable for multilayered systems. However, both their expressions require laborious numerical solutions. On the other hand, Carslaw and Jaeger¹³ provided analytical expressions of the maximum and average temperature rise of the isotropic semi-infinite solid with the rectangular strip supplying a constant surface heat flux:

$$\Delta T_{\max} = \frac{A_0}{\pi L k} \left(\sinh^{-1} \beta + \beta \sinh^{-1} \frac{1}{\beta} \right) \quad (3)$$

$$\Delta T_{\text{ave}} = \frac{A_0}{\pi L k} \left(\sinh^{-1} \beta + \beta \sinh^{-1} \frac{1}{\beta} + \frac{1}{3} \left(\beta^2 + \frac{1}{\beta} - \frac{1}{\beta} (1 + \beta^2)^{\frac{3}{2}} \right) \right), \quad (4)$$

where $\beta = L/b$ and $\sinh^{-1}(x) = \ln(x + \sqrt{x^2 + 1})$. This expression is useful to estimate the steady-state temperature rise in 3ω experiments. However, it still needs to be extended to more sophisticated cases of multilayered systems where the substrates could have anisotropic thermal conductivity tensors.

The need of a generally useful formula to estimate the temperature rise of anisotropic multilayered systems becomes more urgent, especially in recent years with both the thermoreflectance and 3ω methods being developed and extensively used to measure anisotropic thermal conductivities of thin films and bulk materials.¹⁴⁻²⁷ In this work, we accurately solve the heat diffusion equation in the frequency domain and derive a general formalism of the temperature rise of 3D anisotropic multilayered systems in both the thermoreflectance and 3ω experiments, with the aim of providing simple and useful analytical expressions that enable quick and reliable estimation of the peak temperature rise. Such analytical expressions of the peak temperature rise should benefit the design of thermoreflectance and 3ω experiments in choosing the appropriate heating power and heater size for the experiments.

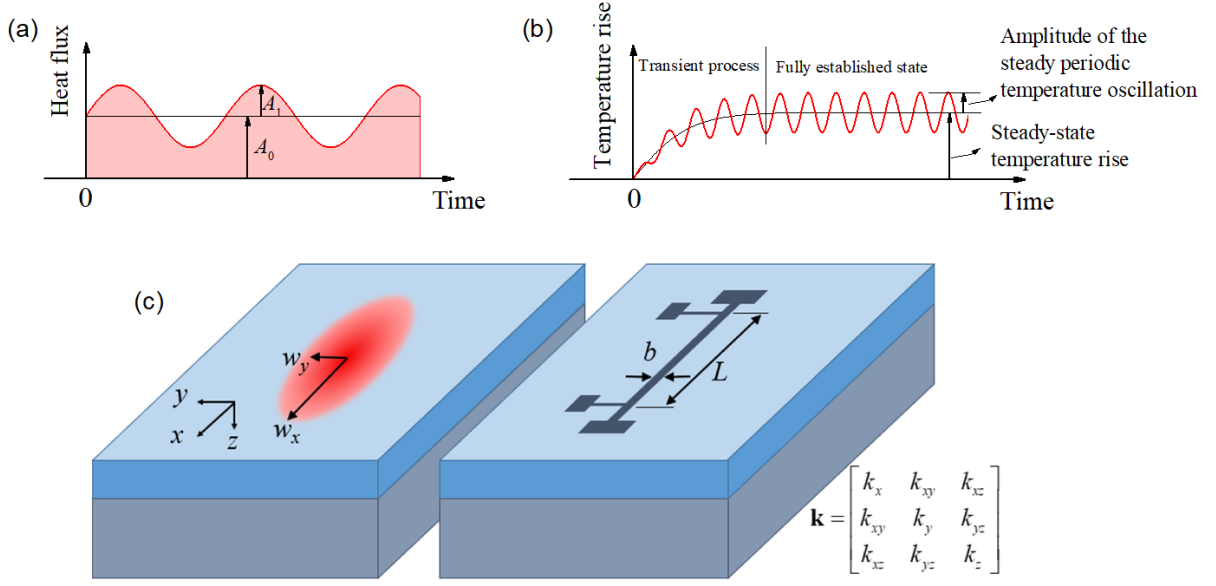


FIG. 1. (a, b) Periodic heat flux with a constant offset generally applied in thermoreflectance and 3ω experiments and the resulted surface temperature rise. (c) Schematic of multilayered sample structures in thermoreflectance and 3ω experiments.

2. General formalism

The studied anisotropic layered systems are illustrated in Fig. 1 (c) for the cases of elliptical laser beam heating and metal strip heating. The governing equation of heat diffusion for each layer of the homogeneous but anisotropic media is:

$$C \frac{\partial T}{\partial t} = k_x \frac{\partial^2 T}{\partial x^2} + k_y \frac{\partial^2 T}{\partial y^2} + k_z \frac{\partial^2 T}{\partial z^2} + 2k_{xy} \frac{\partial^2 T}{\partial x \partial y} + 2k_{xz} \frac{\partial^2 T}{\partial x \partial z} + 2k_{yz} \frac{\partial^2 T}{\partial y \partial z} \quad (5)$$

Here C is the volumetric heat capacity, and $k_x, k_y, k_z, k_{xy}, k_{yz}, k_{xz}$ are the 6 independent components of the 2nd rank thermal conductivity tensor, which must be symmetric due to the constraints by the classical continuum mechanics.^{28, 29} The temperature dependence of the thermophysical properties is ignored for the sake of simplicity. This parabolic partial differential equation can be solved in the frequency domain using a quadrupole approach, details of which can be found in Refs. [16, 20], and the key results are used here.

In the frequency domain, the temperature Θ and the heat flux Q in the i -th layer at depth z_i can be related to those on its surface through the transfer matrix $[M]_i$ as:

$$\begin{bmatrix} \Theta \\ Q \end{bmatrix}_{i,z_i} = [M]_i \begin{bmatrix} \Theta \\ Q \end{bmatrix}_{i,z_i=0} \quad (6)$$

$$[M]_i = \begin{bmatrix} \frac{-u^- \exp(u^+ z_i) + u^+ \exp(u^- z_i)}{(u^+ - u^-)} & \frac{1 - \exp(u^+ z_i) + \exp(u^- z_i)}{k_z (u^+ - u^-)} \\ k_z \frac{u^+ u^- \exp(u^+ z_i) - u^+ u^- \exp(u^- z_i)}{(u^+ - u^-)} & \frac{u^+ \exp(u^+ z_i) - u^- \exp(u^- z_i)}{(u^+ - u^-)} \end{bmatrix}_i, \quad (7)$$

where u^+, u^- are the roots of the equation $x^2 + \lambda_2 x - \lambda_1 = 0$:

$$u^\pm = \frac{-\lambda_2 \pm \sqrt{(\lambda_2)^2 + 4\lambda_1}}{2}, \quad (8)$$

with

$$\lambda_1 \equiv \frac{iC\omega}{k_z} + \frac{4\pi^2 (k_x u^2 + 2k_{xy} uv + k_y v^2)}{k_z}, \quad (9a)$$

$$\lambda_2 \equiv 2i2\pi \frac{(k_{xz} u + k_{yz} v)}{k_z}. \quad (9b)$$

For heat flow across the interface, the Θ and Q on the surface of the second layer can be related to those at the bottom of the first layer as

$$\begin{bmatrix} \Theta \\ Q \end{bmatrix}_{i+1,z_{i+1}=0} = [R] \begin{bmatrix} \Theta \\ Q \end{bmatrix}_{i,z_i=d_i} \quad (10)$$

$$[R] = \begin{bmatrix} 1 & -1/G \\ 0 & 1 \end{bmatrix}, \quad (11)$$

where d_i is the thickness of the i -th layer, and G is the interface thermal conductance.

Note that in the limit $z_i \rightarrow 0$, there is $\exp(u^\pm z_i) \approx 1 + u^\pm z_i$. Therefore, Eq. (7) can be simplified as

$$[M]_i = \begin{bmatrix} 1 & -\frac{z_i}{k_z} \\ k_z u^+ u^- z_i & 1 \end{bmatrix} \approx \begin{bmatrix} 1 & -\frac{z_i}{k_z} \\ 0 & 1 \end{bmatrix}. \quad (12)$$

Equation (12) implies that the interface thermal conductance G can be approximated by an infinitely thin layer with thickness z_i and thermal conductivity k_z , so that $G = k_z/z_i$.

In the other limit $z_i \rightarrow \infty$, there is $e^{u^- z_i} \rightarrow 0$. Therefore, the transfer matrix for the semi-infinite substrate can be simplified as

$$[M]_n = \frac{e^{u^+ d_n}}{(u^+ - u^-)} \begin{bmatrix} -u^- & -\frac{1}{k_z} \\ k_z u^+ u^- & u^+ \end{bmatrix}_n. \quad (13)$$

The Θ and Q at the bottom of the semi-infinite substrate can thus be related to those on the surface of the top layer as

$$\begin{bmatrix} \Theta \\ Q \end{bmatrix}_{n, z_n = d_n} = [M]_n \cdots [M]_2 [M]_1 \begin{bmatrix} \Theta \\ Q - Q_{\text{loss}} \end{bmatrix}_{1, z_1 = 0} = \begin{bmatrix} A & B \\ C & D \end{bmatrix} \begin{bmatrix} \Theta \\ Q - h\Theta \end{bmatrix}_{1, z_1 = 0}, \quad (14)$$

where $Q_{\text{loss}} = h\Theta$, with h [W/m²K] being the heat loss coefficient. Applying the boundary condition that the heat flux at the bottom of the substrate is zero, there is $0 = C\Theta_s + D(Q_s - h\Theta_s)$. The surface temperature response function \hat{G}_s , which is defined as the ratio of the surface temperature to the supplied heat flux, is thus found out as

$$\hat{G}_s(u, v, \omega) \equiv \frac{\Theta_s}{Q_s} = -\frac{D}{C - hD}. \quad (15)$$

After \hat{G}_s is determined, one can then obtain the temperature response function within the i -th layer at position z_i as

$$\begin{bmatrix} \Theta \\ Q \end{bmatrix}_{i, z_i} = [M]_i \cdots [M]_2 [M]_1 \begin{bmatrix} \Theta \\ Q - Q_{\text{loss}} \end{bmatrix}_{1, z_1 = 0} = \begin{bmatrix} T_{11} & T_{12} \\ T_{21} & T_{22} \end{bmatrix} \begin{bmatrix} \Theta \\ Q - h\Theta \end{bmatrix}_{1, z_1 = 0} \quad (16)$$

$$\hat{G}_{i, z_i}(u, v, \omega) \equiv \frac{\Theta_{i, z_i}}{Q_s} = (T_{11} - hT_{12})\hat{G}_s + T_{12}. \quad (17)$$

The next step is to derive the heat flux profile in the frequency domain. For the case of Gaussian profile laser heating, which is commonly encountered in TDTR and FDTR, the surface heat flux is

$$p(x, y, t) = \frac{2}{\pi w_x w_y} \exp\left(-\frac{2x^2}{w_x^2}\right) \exp\left(-\frac{2y^2}{w_y^2}\right) [A_0 + A_1 \exp(\omega_0 t)] u(t), \quad (18)$$

where A_0 and A_1 are the amplitudes of the constant offset and the periodic heating power absorbed by the sample, w_x and w_y are the $1/e^2$ radii of the laser spot in the x and y directions, respectively, ω_0 is the modulation frequency, and $u(t)$ is the unit step function representing the heat flux being switched on after $t \geq 0$. Since we are mainly interested in the steady temperature rise of the system in the fully established state, we can ignore the unit step function in our analysis. Fourier transform of $p(x, y, t)$ gives the frequency-domain heat flux profile as

$$P(u, v, \omega) = 2\pi P_0(u, v) [A_0 \delta(\omega) + A_1 \delta(\omega - \omega_0)], \quad (19a)$$

$$P_0(u, v) = \exp\left(-\frac{\pi^2 u^2 w_x^2}{2}\right) \exp\left(-\frac{\pi^2 v^2 w_y^2}{2}\right). \quad (19b)$$

Similarly, for the case of metal strip electric heating, which is commonly encountered in 3ω experiments, the surface heat flux is

$$p(x, y, t) = \frac{1}{Lb} \Pi\left(\frac{x}{L}\right) \Pi\left(\frac{y}{b}\right) [A_0 + A_1 \exp(\omega_0 t)], \quad (20)$$

where L and b are the length and the width of the rectangular metal strip, respectively, $\Pi(x)$ is the rectangular function, and ω_0 is the frequency of the heat flux (note that the heat flux frequency is twice that of the current frequency due to joule heating). Fourier transform of $p(x, y, t)$ is

$$P(u, v, \omega) = 2\pi P_0(u, v) [A_0 \delta(\omega) + A_1 \delta(\omega - \omega_0)], \quad (21a)$$

$$P_0(u, v) = \text{sinc}(uL) \text{sinc}(vb). \quad (21b)$$

Here the sinc function is defined as $\text{sinc}(t) = \sin(\pi t) / \pi t$.

The temperature response as a result of the surface heating is simply the product of the temperature response function $\hat{G}_{i,z_i}(u,v,\omega)$ and the surface heating profile $P(u,v,\omega)$ in the frequency domain. The real space distribution of the temperature rise in the layered structure can be obtained by doing inverse 2D Fourier transform

$$\begin{aligned}\theta(x, y, z, t) &= \frac{1}{2\pi} \int_{-\infty}^{\infty} \int_{-\infty}^{\infty} \int_{-\infty}^{\infty} P(u, v, \omega) \hat{G}_{i,z}(u, v, \omega) \exp(i2\pi(ux + vy) + i\omega t) du dv d\omega \quad (22) \\ &= A_0 \int_{-\infty}^{\infty} \int_{-\infty}^{\infty} P_0(u, v) \hat{G}_{i,z}(u, v, 0) \exp(i2\pi(ux + vy)) du dv \\ &\quad + A_1 \int_{-\infty}^{\infty} \int_{-\infty}^{\infty} P_0(u, v) \hat{G}_{i,z}(u, v, \omega_0) \exp(i2\pi(ux + vy) + i\omega_0 t) du dv \quad (23)\end{aligned}$$

Equation (23) is one of the key results of this work. The first term in Eq. (23) is a real number, which is the steady-state temperature rise induced by the constant offset of the heat flux. The second term in Eq. (23) is a complex number, which is the steady periodic temperature oscillation induced by the periodic surface heat flux.

The integrals in Eq. (23) generally need to be evaluated numerically. Note that one should take great care to choose an accurate and robust numerical method for the integration. Sufficiently dense grids should be chosen especially around the origin ($u=v=0$). We found that the Gauss-Legendre method for integration, while being computationally efficient, fails to work well at low frequencies $\frac{\omega_0}{2\pi} < 10$ kHz, where the in-plane thermal diffusion length $d_{f,r} = \sqrt{2k_r/\omega_0 C}$ could be much larger than the heater size, placing a requirement on the smallest grid size ($\propto 1/d_{f,r}$) that should be used around the origin. Here we use the trapezoidal rule with a non-uniform grid for the integration, with the grid size increasing logarithmically from the center of the integration domain. Grid-independence study was conducted to ensure that converged results were obtained. The upper limit of the integral can be set as $2/w_x$ and $2/w_y$ ($4/L$ and $4/b$ for the case of metal strip heating) for u and v , respectively, without losing much accuracy.

This general formalism of the steady-state temperature rise in 3D anisotropic multilayered systems for both laser heating and metal strip joule heating has been implemented in MATLAB code, which is available in Supplementary Information.

3. Analytical expressions of the temperature rise in semi-infinite solids

The general formalism derived above, while being accurate within the assumption of constant thermophysical properties, requires complicated numerical coding. One may wish to derive some simple analytical expressions to assist quick estimations of the temperature rise in experiments. This is possible for some simple cases, such as the semi-infinite solid with an orthogonal thermal conductivity tensor ($k_{xy} = k_{xz} = k_{yz} = 0$), for which the surface temperature response function (Eq. (15)) can be specifically expressed out as

$$\hat{G}_s(u, v, \omega) = \frac{1}{h + \sqrt{iC\omega k_z + 4\pi^2 k_z (k_x u^2 + k_y v^2)}}. \quad (24)$$

In what follows, the temperature rise in the semi-infinite solid induced by the constant and periodic heat flux are analyzed separately for both laser heating and metal strip heating.

3.1 Steady-state temperature rise induced by the constant heat flux

For the case of laser heating on the surface of a semi-infinite solid, the highest steady-state temperature rise is located at $x = y = z = 0$ and expressed as:

$$\theta_{\max} = \int_{-\infty}^{\infty} \int_{-\infty}^{\infty} \frac{A_0 \exp\left(-\frac{\pi^2 u^2 w_x^2}{2}\right) \exp\left(-\frac{\pi^2 v^2 w_y^2}{2}\right)}{h + 2\pi \sqrt{k_z (k_x u^2 + k_y v^2)}} du dv. \quad (25)$$

Equation (25) still needs to be evaluated numerically. However, it can further simplified for the case of in-plane symmetry with $w_x = w_y = w_0$ and $k_x = k_y = k_r$, and with zero heat loss $h = 0$:

$$\theta_0 = \int_0^{\infty} \frac{A_0}{\sqrt{k_z k_r}} \exp\left(-\pi^2 w_0^2 \rho^2 / 2\right) d\rho = \frac{A_0}{\sqrt{2\pi w_0^2 k_z k_r}}. \quad (26)$$

This result is identical with Eq. (1) if the probe laser spot size w_1 in Eq. (1) is set as 0. This is because the temperature rise derived here is the peak value induced by the pump heating and is independent of the probe beam, whereas the temperature rise derived by Cahill⁹ and Braun *et al.*¹⁰ was the value averaged by the Gaussian profile of the probe beam. In the limit $w_1 \rightarrow 0$, the probe beam detects only the peak temperature induced by the pump heating.

For the in-plane anisotropic cases, corrections are needed based on the thermal conductivity anisotropy $\alpha = \sqrt{k_y/k_x}$ and the spot size anisotropy $\beta = w_y/w_x$. Setting $k_r = \sqrt{k_x k_y}$ and $w_0 = \sqrt{w_x w_y}$, we have the steady-state temperature rise of the semi-infinite solid with in-plane anisotropy and zero heat loss as

$$\theta_{\max} = \xi \frac{A_0}{\sqrt{2\pi w_x w_y k_z \sqrt{k_x k_y}}}, \quad (27)$$

$$\xi = \frac{w_0}{\sqrt{2\pi}} \int_{-\infty}^{\infty} \int_{-\infty}^{\infty} \frac{\exp[-\pi^2 w_0^2 (u^2/\beta + \beta v^2)/2]}{\sqrt{(u^2/\alpha + \alpha v^2)}} du dv. \quad (28)$$

The correction factor ξ is a function of solely α/β and is plotted out in Fig. 2(a). Note that although Eq. (28) contains w_0 explicitly, its effect is essentially cancelled out, and thus ξ is independent of w_0 .

For the case of metal strip heating, assuming zero heat loss, the highest steady-state temperature rise of the semi-infinite solid is expressed as:

$$\theta_{\max} = \int_{-\infty}^{\infty} \int_{-\infty}^{\infty} \frac{A_0 \operatorname{sinc}(uL) \operatorname{sinc}(vb)}{2\pi \sqrt{k_z} \sqrt{k_x u^2 + k_y v^2}} du dv \quad (29)$$

$$= \psi \frac{A_0}{\pi L \sqrt{k_z k_x}}, \quad (30)$$

where the correction factor due to in-plane anisotropy is expressed as

$$\begin{aligned}\psi &= \int_{-\infty}^{\infty} \int_{-\infty}^{\infty} \text{sinc}(u) \text{sinc}(v) \frac{\alpha\beta}{2\sqrt{u^2 + \alpha^2\beta^2v^2}} dudv \\ &= \sinh^{-1}(\alpha\beta) + \alpha\beta \sinh^{-1}\left(\frac{1}{\alpha\beta}\right)\end{aligned}\quad (31)$$

Here $\alpha = \sqrt{k_y/k_x}$, $\beta = L/b$, and $\sinh^{-1}(x) = \ln(x + \sqrt{x^2 + 1})$. The correction factor ψ as a function of $\alpha\beta$ is plotted in Fig. 2(b). Note that by setting $k_x = k_y = k_z$, Eq. (30) reduces exactly to Eq. (3), the analytical expression provided by Carslaw and Jaeger.¹³

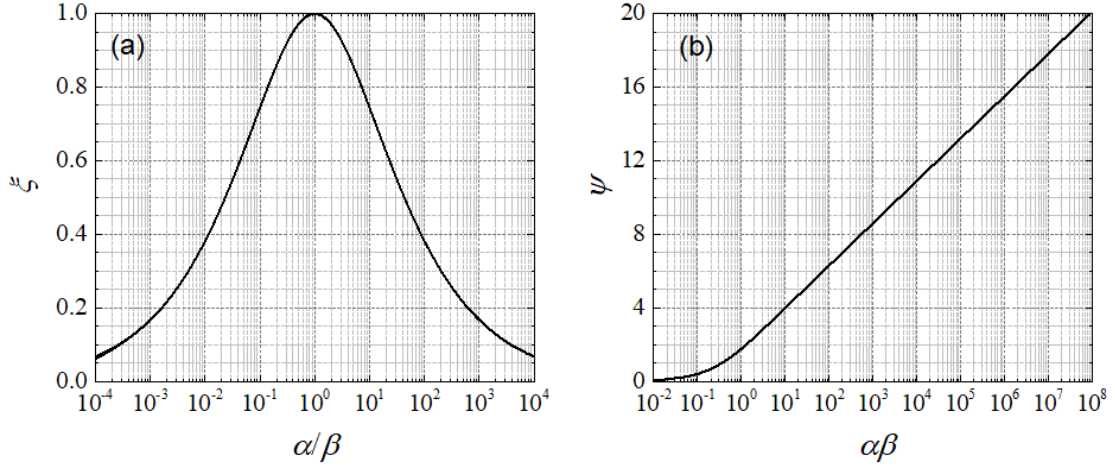


FIG. 2. (a) The correction factors ξ (as expressed in Eq. (28)) for the steady-state temperature rise of semi-infinite solids under constant laser heating as a function of α/β , with $\alpha = \sqrt{k_y/k_x}$ and $\beta = w_y/w_x$. (b) The correction factor ψ (as expressed in Eq. (31)) for the steady-state temperature rise of semi-infinite solids under constant electric heating as a function of $\alpha\beta$, with $\alpha = \sqrt{k_y/k_x}$ and $\beta = L/b$.

Equations (27) and (30) suggest that the steady-state temperature rise of the semi-infinite solid is proportional to both the heat flux and the square-root of the heated area, $\theta \propto \frac{q''}{k} \sqrt{A}$, here A is the heated area. Therefore, with a finite heated area, the steady-state temperature rise could always be established due to the heat sink effect of the semi-infinite solid, even when the heat loss is zero. On the other hand, for the case of 1D uniform heating with an infinitely large heated area, the surface temperature rise given by Carslaw and Jaeger³⁰ as $\theta(z=0) = \frac{2q''}{k} \sqrt{\frac{kt}{\pi c}} \propto \sqrt{t}$, where t is the heating time, would approach infinity and a steady state could never be established.

3.2 Periodic temperature oscillation induced by the periodic heat flux

When the heating frequency ω_0 is nonzero, the temperature rise θ would be a complex number, with the real and imaginary parts oscillating with time but the amplitude being constant in the fully established state. To understand how the heating frequency affects the amplitude of the steady periodic temperature oscillation, we plot in Fig. 3 the ratio of the amplitude of the periodic temperature oscillation at different heating frequencies to the steady-state temperature rise, with the constant and periodic heat flux having the same amplitudes. We find that the temperature ratios mainly depend on the ratio between the in-plane thermal diffusion length and the heater size. Here the averaged in-plane thermal diffusion length $d_{f,r} = \sqrt{2k_r/\omega_0 C}$ is defined using the averaged in-plane thermal conductivity $k_r = \sqrt{k_x k_y}$. The characteristic length of the heater size can be the average laser spot size w_0 defined as $w_0 = \sqrt{w_x w_y}$ for the case of laser heating and the metal strip length L for the case of metal strip heating.

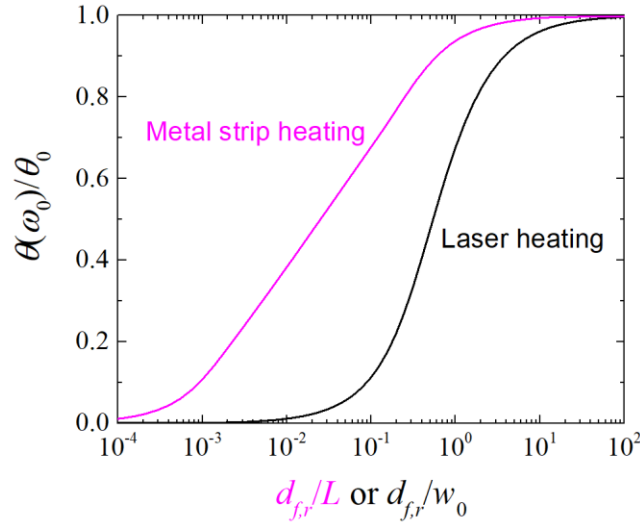


FIG. 3. The ratio of the amplitude of the periodic temperature oscillation to the steady-state temperature rise of the semi-infinite solid under the same amplitude of heating power, plotted as a function of in-plane thermal diffusion length normalized by the heater size. The curve for the metal strip heating is plotted for the specific case of $k_x = k_y$ and $L/b > 1000$, and the curve for the laser heating is plotted for the specific case of $\sqrt{k_y/k_x} = w_y/w_x$. The curves for other cases could be slightly different.

Figure 3 suggests that the amplitude of the steady periodic temperature oscillation of a semi-infinite bulk material is always less than or equal to its steady-state temperature rise under the same amplitude of heating power, determined by the ratio of the in-plane heat diffusion length and the heater size. When $d_{f,r} \gg w_0$ (or L), which can be met by setting the heating frequency $\omega_0 \rightarrow 0$, the amplitude of the periodic temperature oscillation approaches the steady-state temperature rise. On the other hand, when $d_{f,r} \ll w_0$ (or L), the amplitude of the periodic temperature oscillation approaches zero. This suggests that the periodic signals would reduce at higher modulation frequencies and larger laser spot sizes even under the same intensity of heating power, which is consistent with experimental observations.

The trend shown in Fig. (3) should apply to layered structures as well. We thus only need to estimate the steady-state temperature rise and make sure that it is not too high; we are then certain that the amplitude of the periodic temperature oscillation due to the periodic heating will be within the acceptable range. Note that the steady-state temperature rise depends only on the thermal conductivity but not on the heat capacity of the material. Therefore, the heat capacity of the material does not place any constraint on the temperature rise in FDTR and 3ω experiments. The situation, however, is different in TDTR experiments, where pulsed laser is used for the heating. From a simple analysis using the lumped capacitance method,³¹ the temperature excursion on the surface of the metal film transducer in TDTR should be $\theta = q''/Cd$ immediately after the pulse heating, followed by an exponential decay with a thermal time constant $\tau \propto Cd$. Here, q'' is the surface heat flux and Cd is the heat capacity of the metal film transducer per unit area. With dramatically reduced heat capacities of materials at low temperatures <30 K, the temperature excursion following the pulse heating will be exceptionally high, limiting the average laser power used and thus constraint the applicability of TDTR at low temperatures.^{6, 8}

The above analysis assumed zero heat loss. Additional heat loss would reduce the temperature rise. The effect of heat loss on the reduction of the temperature rise is determined by the Biot number. For the steady-state temperature rise, the Biot number is defined as $Bi = hL_c/\sqrt{k_z k_r}$, where L_c is the characteristic length of the heater size ($L_c = w_0$ for laser heating and $L_c = L$ for metal strip heating). For the periodic temperature oscillation, another Biot number can be defined as $Bi = h d_{f,z}/k_z$, where $d_{f,z} = \sqrt{2k_z/\omega_0 C}$ is the through-plane thermal diffusion length. The reason for choosing the different characteristic length scales in the definitions of the Biot number can be manifested by analyzing Eq. (24). The general rule is that with $Bi \ll 1$, the temperature rise in the solid is little affected by the heat loss; with $Bi \geq 1$, the temperature rise is significantly reduced compared to the case without any heat loss.

4. Analytical expressions of the temperature rise in layered structures

The case of multilayered systems could be more complicated than the semi-infinite solid mainly because the layers above the semi-infinite substrate could redistribute the heat flux in the multilayered media, making the heat flux profiles on the surfaces of the subsequent layers different from the one originally applied on the surface of the first layer. However, with the assumptions that the heat flux profile is constant throughout the layers and that the temperature gradient across the thin films is linear, the steady-state temperature rise across the multilayered structure can be estimated as:

$$\Delta T = \sum_{i=1}^{n-1} \frac{2A_0}{\pi w_x w_y} \left(\frac{d_i}{k_{z,i}} + \frac{1}{G_i} \right) + \xi \frac{A_0}{\sqrt{2\pi w_x w_y k_{z,n} \sqrt{k_{x,n} k_{y,n}}}} \quad (32)$$

for the case of laser heating, and

$$\Delta T = \sum_{i=1}^{n-1} \frac{A_0}{Lb} \left(\frac{d_i}{k_{z,i}} + \frac{1}{G_i} \right) + \psi \frac{A_0}{\pi L \sqrt{k_{z,n} k_{x,n}}} \quad (33)$$

for the case of metal strip heating, where ξ and ψ are correction factors that have been expressed in Eqs. (28) and (31) and can also be directly read from Fig. 2 (a, b), respectively.

In what follows, we will study three cases of two-layered systems with the substrate having thermal conductivities 1) much higher than, 2) much lower than, and 3) similar to the ones of the layer above. We will use the analytical expressions Eqs. (32) and (33) for quick estimations of the steady-state temperature rise of these anisotropic layered structures and compare them with numerical solutions of the general formalism outlined in Section II to see how accurate these analytical expressions could be for the different cases.

The properties of the two-layered systems for the three cases are tabulated in Table I. The three cases mainly differ from each other in their heat sink locations: whether the heat sink is in the substrate, the top layer, or both. The first two cases were purposefully chosen to be 3D anisotropic whereas the third one was chosen to be isotropic to test the general applicability of the analytical expressions. The interface thermal conductance is assumed to be $G=100$ MW/m²K for all the three cases. For the case of laser heating, the laser spot is assumed to be elliptical, with $w_x = 20$ μ m and $w_y = 5$ μ m. For the case of metal strip heating, the metal strip dimension is assumed to be $L=1$ mm and $b=10$ μ m, with the metal strip aligned along the x -direction. The heating power for each case, adjusted to result in the similar temperature rise among the different cases, is also listed in Table I.

Figure 4 compares the estimated temperature rises using the analytical expressions (bars with patterns) with the accurate solutions of the general formalism (bars without patterns) for the three cases for both laser heating and metal strip heating. The total temperature rise is the sum of contributions from three components: the first layer (the white area on the top of the bar), the interface (the black area in the middle of the bar), and the substrate (the grey area at the bottom of the bar). The results show that the temperature rise contributed by the top layer and the interface can be estimated well using the analytical expressions. The estimations by

the analytical expressions mainly differ from the accurate numerical results on the temperature rise of the semi-infinite substrate. The analytical expressions work very well for cases 1 and 3, where the substrate has a thermal conductivity similar to or higher than the in-plane thermal conductivity of the first layer, resulting in insignificant in-plane heat spreading within the first layer. For case 2, however, the analytical expressions overestimate the temperature rise by 30% for metal strip heating and 125% for laser heating. This is because in case 2, the first layer has an in-plane thermal conductivity much higher than that of the substrate, contributing a significant radial heat sink effect.

TABLE I. Parameters of three cases studied to estimate temperature rise

		k_x	k_y	k_z	d (nm)	A (mW)	
		(W/mK)	(W/mK)	(W/mK)		Laser	Metal strip
Case 1	Layer 1	50	10	5	100	15	300
	Substrate	1000	2000	1	inf		
Case 2	Layer 1	500	200	5	100	2	20
	Substrate	10	5	1	inf		
Case 3	Layer 1	200	200	200	100	50	1000
	Substrate	160	160	160	inf		

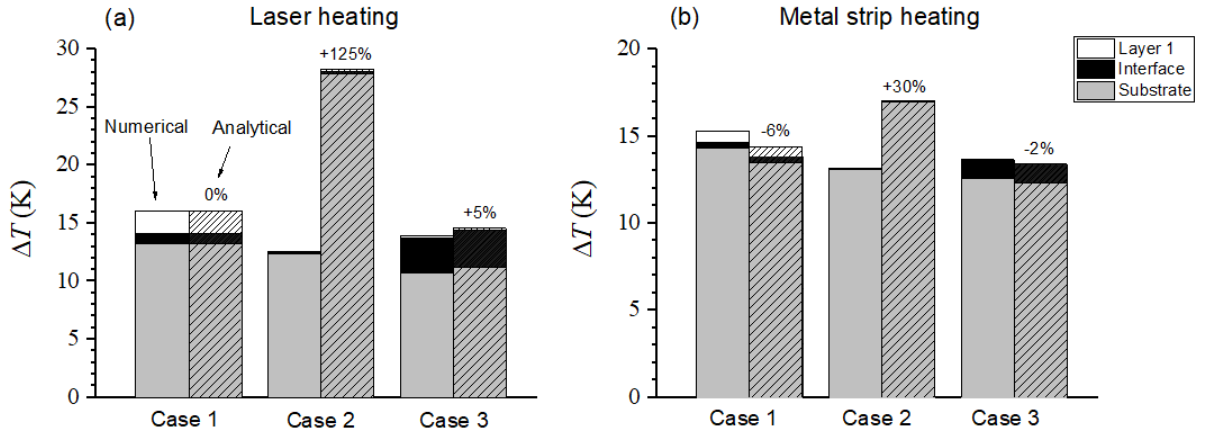


FIG. 4. Comparison of the temperature rise of three cases of two-layered systems calculated numerically (bars without patterns) and analytically (bars with patterns) under (a) laser heating and (b) metal strip heating. In the bars, the white areas are the temperature rise contributed by the thin layer, the black areas are the one contributed by the interface, and the gray areas are the one contributed by the substrate.

The general effect of the radial heat sink in the layers above the substrate is to spread out the heat flux and reduce the peak amplitude of the heat flux on the substrate, resulting in a

reduced temperature rise than the estimated value. Besides, if the films were too thick to have a linear temperature gradient across the films, the actual temperature rise would also be smaller than the estimated. However, it is always better to err on the side of caution. Since in both cases the analytical expressions over-estimate the temperature rise, they still serve the purpose of making sure the temperature rise is not too high in the experiments. For occasions where the temperature rise needs to be known more precisely, one can always refer to the general formalism outlined in Section II for a more accurate calculation.

5. Conclusions

This work provided simple analytical expressions for quick and accurate estimation of the peak steady-state temperature rise in 3D anisotropic layered systems in thermoreflectance and 3ω experiments. The 3D anisotropic heat diffusion equation has been solved first in the frequency domain to derive a general formalism of the temperature rise in multilayered systems, from which specific analytical expressions are derived to calculate the peak temperature rise of an anisotropic semi-infinite solid. The analytical expressions are then extended to the case of multilayered systems. By comparing with the accurate numerical solutions of the heat diffusion equation, these analytical expressions are found to work well for most cases. In some special occasions such as when the layers above the substrate have significant radial heat sink effect, the temperature rise could be overestimated. These simple analytical expressions serve the purpose of estimating the maximum temperature rise of 3D anisotropic layered systems, which greatly benefits the FDTR/TDTR and 3ω experiments in choosing an appropriate set of heating power and heater size for the experiments.

Supplementary information

The MATLAB code package for the temperature rise of 3D anisotropic layered systems under elliptical laser beam heating and metal strip joule heating, with the model derivation outlined in Section II, is available at <https://github.com/jiangpq04/Temperature-rise>

Acknowledgments

P.J. acknowledges the financial support by the R.K. Mellon Postdoctoral Fellowship.

References:

1. E. Machlin, *Materials Science in Microelectronics I: The Relationships Between Thin Film Processing and Structure*. (Elsevier Science, 2010).
2. F. Bonaccorso, Z. Sun, T. Hasan and A. C. Ferrari, *Nature Photonics* **4** (9), 611-622 (2010).
3. Y. Hamakawa, *Thin-film solar cells: next generation photovoltaics and its applications*. (Springer Science & Business Media, 2013).
4. N. P. Padture, M. Gell and E. H. Jordan, *Science* **296** (5566), 280-284 (2002).
5. M. S. Dresselhaus, G. Chen, M. Y. Tang, R. G. Yang, H. Lee, D. Z. Wang, Z. F. Ren, J. P. Fleurial and P. Gogna, *Adv. Mater.* **19** (8), 1043-1053 (2007).
6. P. Jiang, X. Qian and R. Yang, *J. Appl. Phys.* **124** (16), 161103 (2018).
7. C. Dames, *Annu. Rev. Heat Transfer* **16** (16), 7 (2013).
8. D. G. Cahill, P. V. Braun, G. Chen, D. R. Clarke, S. Fan, K. E. Goodson, P. Keblinski, W. P. King, G. D. Mahan, A. Majumdar, H. J. Maris, S. R. Phillpot, E. Pop and L. Shi, *Appl. Phys. Rev.* **1** (1), 011305 (2014).
9. D. G. Cahill, *Rev. Sci. Instrum.* **75** (12), 5119 (2004).
10. J. L. Braun, C. J. Szwejkowski, A. Giri and P. E. Hopkins, *J. Heat Transfer* **140** (5), 052801 (2018).
11. D. G. Cahill, *Rev. Sci. Instrum.* **61** (2), 802 (1990).
12. T. Borca-Tasciuc, A. R. Kumar and G. Chen, *Rev. Sci. Instrum.* **72** (4), 2139 (2001).
13. H. S. Carslaw and J. C. Jaeger, (Clarendon Press, 1959), Page 265.
14. A. T. Ramu and J. E. Bowers, *Rev. Sci. Instrum.* **83** (12), 124903 (2012).
15. J. P. Feser and D. G. Cahill, *Rev. Sci. Instrum.* **83** (10), 104901 (2012).
16. J. P. Feser, J. Liu and D. G. Cahill, *Rev. Sci. Instrum.* **85** (10), 104903 (2014).
17. V. Mishra, C. L. Hardin, J. E. Garay and C. Dames, *Rev. Sci. Instrum.* **86** (5), 054902 (2015).
18. D. Rodin and S. K. Yee, *Rev. Sci. Instrum.* **88** (1), 014902 (2017).
19. P. Jiang, X. Qian and R. Yang, *Rev. Sci. Instrum.* **88** (7), 074901 (2017).
20. P. Jiang, X. Qian and R. Yang, *Rev. Sci. Instrum.* **89** (9), 094902 (2018).
21. P. Jiang, X. Qian, X. Li and R. Yang, *Appl. Phys. Lett.* **113** (23), 232105 (2018).
22. M. Li, J. S. Kang and Y. Hu, *Rev. Sci. Instrum.* **89** (8), 084901 (2018).
23. M. Rahman, M. Shahzadeh, P. Braeuninger-Weimer, S. Hofmann, O. Hellwig and S. Pisana, *J. Appl. Phys.* **123** (24), 245110 (2018).
24. P. Jiang, X. Qian, X. Gu and R. Yang, *Adv. Mater.* **29** (36), 1701068 (2017).
25. X. Qian, P. Jiang and R. Yang, *Materials Today Physics* **3**, 70-75 (2017).
26. P. Jiang, X. Qian, R. Yang and L. Lindsay, *Physical Review Materials* **2** (6), 064005 (2018).
27. X. Qian, P. Jiang, P. Yu, X. Gu, Z. Liu and R. Yang, *Appl. Phys. Lett.* **112** (24), 241901 (2018).
28. J. M. Powers, *J. Heat Transfer* **126** (5), 670-675 (2004).
29. A. R. Hadjesfandiari, *International Journal of Materials and Structural Integrity* **8** (4), 209-220 (2014).
30. H. S. Carslaw and J. C. Jaeger, *Conduction of heat in solids*. (Clarendon Press, 1959), Page 75.

31. T. L. Bergman, A. S. Lavine, F. P. Incropera and D. P. DeWitt, *Fundamentals of Heat and Mass Transfer*. (Wiley, 2017), Page 254.